

Nematic topological semimetal and insulator in magic angle bilayer graphene at charge neutrality

Shang Liu, Eslam Khalaf, Jong Yeon Lee, and Ashvin Vishwanath

Department of Physics, Harvard University, Cambridge, MA 02138

(Dated: November 30, 2021)

We report on a fully self-consistent Hartree-Fock calculation of interaction effects on the Moiré flat bands of twisted bilayer graphene, assuming that valley U(1) symmetry is respected. We use realistic band structures and interactions and focus on the charge neutrality point, where experiments have variously reported either insulating or semimetallic behavior. Restricting the search to orders for which the valley U(1) symmetry remains unbroken, we find three types of self-consistent solutions with competitive ground state energy (i) insulators that break $C_2\mathcal{T}$ symmetry, including valley Chern insulators (ii) spin or valley polarized insulators and (iii) rotation C_3 symmetry breaking semimetals whose gaplessness is protected by the topology of the Moiré flat bands. We find that the relative stability of these states can be tuned by weak strains that break C_3 rotation. The nematic semimetal and also, somewhat unexpectedly, the $C_2\mathcal{T}$ breaking insulators, are stabilized by weak strain. These ground states may be related to the semi-metallic and insulating behaviors seen at charge neutrality, and the sample variability of their observation. We also compare with the results of STM measurements near charge neutrality.

I. INTRODUCTION

The discovery of interaction-driven insulating and superconducting behavior in twisted bilayer graphene (TBG) [1, 2] has inspired intensive efforts to understand this behavior [3–16] and to find related systems which exhibit similar phenomenology [17–22]. This work has started to bear fruit with several groups announcing similar observations in TBG samples [23–26] as well as other Moiré materials [27–31]. The basic mechanism underlying the enhancement of correlation in these materials is understood to originate from the long-wavelength Moiré pattern leading to quenching of the electron kinetic energy manifested in flat energy bands [32, 33]. Nevertheless, the nature of the observed correlated insulating states remains under debate [4–6, 8, 9].

Early experiments found clear signature of a correlated insulating state at half-filling [34] [1, 23]. Subsequently, insulating ferromagnetic states were also observed at quarter and three-quarter fillings [23, 24]. On the other hand, in all these experiments [1, 2, 23] insulating behavior was absent at charge neutrality (CN) where signatures of semimetallic behavior were observed instead. In contrast, a recent experiment surprisingly found an insulator at CN with a transport gap exceeding those at 1/2, 1/4 and 3/4 fillings [25].

On the theory side, it was realized early on [4, 35] that a simple Mott picture for the insulating phase is complicated by the band topology which prohibits the construction of localized orbitals describing the flat bands while preserving all the symmetries. Various orders have been proposed to account for the insulating states. At charge neutrality, a $C_2\mathcal{T}$ symmetry breaking insulator, with Chern number ± 1 for each spin and valley flavour was proposed in [9], along with a $C_2\mathcal{T}$ symmetry preserving insulator that is believed to require mixing with remote bands [9]. An intervalley coherent order [4] was proposed as a candidate for the insulating state at half-filling while nematic orders were discussed in [6, 11, 36] and ferromagnetic ordering was proposed in [8]. In the presence of explicit C_2 symmetry breaking induced by a substrate, valley or spin polarized insulator with valley resolved Chern numbers have been discussed [17, 37].

In this letter, we perform a self-consistent Hartree-Fock mean field analysis for the screened Coulomb interaction projected onto the flat bands.

We focus on the CN point because of its pivotal role in determining the entire phase diagram. We will discuss other fillings in subsequent work. For simplicity, we restrict our attention to orders that conserve the U(1) valley charge as well as translation invariance at the scale of the Moiré unit cell. Our results include the expected spin-polarized and valley-polarized insulators, which break no other symmetries. In addition we observe a strong tendency to breaking spatial rotation symmetries. We find a $C_2\mathcal{T}$ -breaking insulator and two distinct $C_2\mathcal{T}$ -symmetric semimetallic phases which break C_3 -symmetry. The $C_2\mathcal{T}$ -breaking phase has a Chern number of $C = \pm 1$, per flavor (i.e. valley and spin). Different spin/valley orderings then lead to various ground states ranging from quantum anomalous Hall (QAH) to quantum valley Hall (QVH) or quantum spin Hall (QSH) insulators with very similar Hartree-Fock energies. Of these, the QVH insulator breaks C_2 symmetry, allowing for a direct coupling to the C_2 -breaking hBN substrate, potentially favoring it in situations where the sample and substrate are aligned. The gapless C_3 -breaking phases are obtained by bringing the two Dirac cones from the Moiré K and K' very close to the Γ point. Instead of merging and opening a gap as one might normally expect, the Dirac points remain gapless since they carry the same chirality [4], a consequence of descending from the Dirac points of graphene from the same valley for the two layers. This topological protection prevents them from annihilating, resulting in a gapless semimetallic state. Thus, the metallic nature at CN in this scenario is intimately tied to the topological properties of the magic angle flat bands.

We investigate the effect of small explicit C_3 symmetry breaking which can arise in real samples due to strain [21], and show that it strongly influences the competition between different symmetry broken phases, favoring one of the C_3 -breaking semimetallic phases. Surprisingly, the $C_2\mathcal{T}$ -breaking insulators also exhibits a strong susceptibility to C_3 symmetry breaking. The energies of the insulating $C_2\mathcal{T}$ -breaking and the semimetallic $C_2\mathcal{T}$ -preserving states are low-

ered compared to the spin/valley ferromagnets, and approach each other quickly as the value of the C_3 -breaking parameter is increased. Our results suggest that these two states are candidate ground states in the presence of very small explicit C_3 symmetry breaking which is likely to exist in experiments. Further competition between these two phases is likely to be settled by small sample-dependent details, potentially explaining the realization of an insulator in some samples and a semimetal in other samples.

II. PROBLEM SETUP

The single-particle physics is described by the Bistritzer-MacDonald (BM) model [32, 33], which employs a continuum approximation close to K and K' for a pair of graphene sheets rotated relative to each other by an angle θ . The Hamiltonian for the K valley is given by:

$$\mathcal{H}_+ = \sum_l \sum_{\mathbf{k}} f_l^\dagger(\mathbf{k}) h_{\mathbf{k}}(l\theta/2) f_l(\mathbf{k}) + \left(\sum_{\mathbf{k}} \sum_{i=1}^3 f_i^\dagger(\mathbf{k} + \mathbf{q}_i) T_i f_b(\mathbf{k}) + h.c. \right). \quad (1)$$

Here, $l = t/b \simeq \pm 1$ is the layer index, and $f_l(\mathbf{k})$ is the K -valley electron originated from layer l . $h_{\mathbf{k}}(\theta)$ is the monolayer graphene K -valley Hamiltonian with twist angle θ (see Appendix for details) and \mathbf{q}_1 is defined as $K_b - K_t$ with K_l denoting the K -vector of layer l . $\mathbf{q}_2 = O_3 \mathbf{q}_1$ is the counter-clockwise $2\pi/3$ rotation of \mathbf{q}_1 , and $\mathbf{q}_3 = O_3 \mathbf{q}_2$. Finally, the interlayer coupling matrices are given by

$$T_j = \begin{pmatrix} w_0 & w_1 e^{-(j-1)\frac{2\pi i}{3}} \\ w_1 e^{(j-1)\frac{2\pi i}{3}} & w_0 \end{pmatrix}, \quad (2)$$

with w_0 and w_1 denoting intrasublattice and intersublattice hopping, respectively. Due to lattice relaxation effects, which shrink the AA regions relative to the AB regions, the value of w_0 at the magic angle is about 75% of w_1 [38, 39]. Throughout this work, we will use the values $w_1 = 110$ meV and $w_0 = 82.5$ meV. Explicit C_3 symmetry breaking is implemented via the substitution $T_1 \rightarrow (1 + \beta)T_1$ [40].

To study possible correlated insulating states, we employ a momentum-space self-consistent Hartree-Fock mean field theory. The momentum-space description allows us to focus on the pair of flat bands at CN, thereby evading the difficulties associated with the real space Wannier obstruction rooted in the fragile topology of these bands [4, 35, 41]. Restricting the analysis to the flat bands is only justified in the limit when both the bandwidth and interaction strength are much smaller than the bandgap. For realistic interactions, the interaction strength is of the same order as the bandgap which means that symmetry-broken states involving remote bands cannot be ruled out [9]. However, given the strong angle dependence and appearance of correlated states only near the magic angle [1, 2, 23], it is likely that the relevant symmetry-broken phases experimentally originate mostly from the two flat bands which

justifies our approximation. We note, however, that our approach cannot capture possible changes in the topology of the flat bands arising from mixing with remote bands which were argued to be relevant in Ref. [9].

The Hartree-Fock (HF) mean field theory is defined in terms of the projector

$$P_{\alpha,\beta}(\mathbf{k}) = \langle c_\alpha^\dagger(\mathbf{k}) c_\beta(\mathbf{k}) \rangle, \quad P(\mathbf{k})^2 = P(\mathbf{k}) = P(\mathbf{k})^\dagger, \quad (3)$$

where $c_\alpha(\mathbf{k})$ is the annihilation operator for an electron at momentum \mathbf{k} and $\alpha = (n, \tau, s)$ is a combined index for band, valley and spin, respectively. For a gapped or semimetallic phase at CN, P satisfies $\text{tr } P(\mathbf{k}) = 4$ for all \mathbf{k} points[42]. The HF mean field Hamiltonian has the form

$$\mathcal{H}_{\text{MF}} = \sum_{\mathbf{k}} \{ c(\mathbf{k})^\dagger [h_0(\mathbf{k}) + h_{\text{HF}}(P, \mathbf{k})] c(\mathbf{k}) - \frac{1}{2} \text{tr } h_{\text{HF}}(P, \mathbf{k}) P^T(\mathbf{k}) \}. \quad (4)$$

Here, $c(\mathbf{k})$ is a column vector in the index α , $h_0(\mathbf{k})$ denotes the single particle Hamiltonian and $h_{\text{HF}}(\mathbf{k})$ is given by

$$h_{\text{HF}}(P, \mathbf{k}) = \frac{1}{A} \sum_{\mathbf{G}} V_{\mathbf{G}} \Lambda_{\mathbf{G}}(\mathbf{k}) \sum_{\mathbf{k}'} \text{tr } P^T(\mathbf{k}') \Lambda_{\mathbf{G}}^\dagger(\mathbf{k}') - \frac{1}{A} \sum_{\mathbf{q}} V_{\mathbf{q}} \Lambda_{\mathbf{q}}(\mathbf{k}) P^T(\mathbf{k} + \mathbf{q}) \Lambda_{\mathbf{q}}^\dagger(\mathbf{k}), \quad (5)$$

where A is the total area. The \mathbf{k}' , \mathbf{G} , and \mathbf{q} summations range over the first Brillouin zone, reciprocal lattice vectors, and all momenta, respectively. $V_{\mathbf{q}}$ is the interaction potential which we take to be a single-gate-screened Coulomb interaction $V_{\mathbf{q}} = \frac{e^2}{2\epsilon\epsilon_0 q} (1 - e^{-2qd_s})$ with dielectric constant $\epsilon = 7$ and screening length equal to the gate distance $d_s \approx 40$ nm.

The first term in (5) is the Hartree term while the second is the Fock term. The matrix $\Lambda_{\mathbf{q}}(\mathbf{k})$ contains the form factors for the single-particle

$$[\Lambda_{\mathbf{q}}(\mathbf{k})]_{\alpha,\beta} = \langle u_\alpha(\mathbf{k}) | u_\beta(\mathbf{k} + \mathbf{q}) \rangle. \quad (6)$$

where α and β denote a combined index for spin, valley and band. The HF self-consistent analysis starts by proposing an ansatz for the projector $P(\mathbf{k})$, then substituting in the Hamiltonian (4) which is then used to compute the new projector. This procedure is iterated until convergence is achieved.

One important subtlety in the HF approach is that the band structure depends on the filling even without symmetry breaking. This follows from the fact that the form factor matrix $\Lambda_{\mathbf{q}}(\mathbf{k})$ is not diagonal in the band index for $\mathbf{q} \neq 0$ since the Bloch wavefunctions $u_{\alpha,\mathbf{k}}$ from different bands are not orthogonal at different momenta. In addition, the Hartree term contains a trace over all filled bands which also affects the dispersion of the empty bands. This means that the band structure obtained from the BM model is only valid at a specific filling which determines the references point for our analysis. At this point, it will be assumed that interaction effects are already included in the parameters of the effective model which can

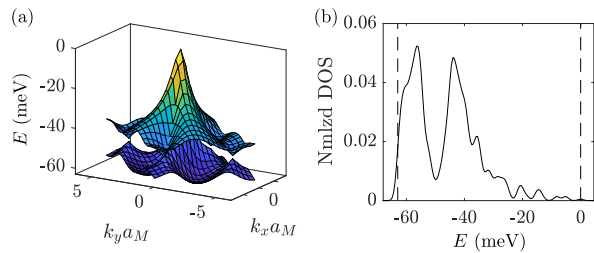


FIG. 1. (a) K -valley band structure at empty filling. (b) Normalized density of states at empty filling, valid for both valleys.

be obtained by fitting to *ab initio* calculations or comparing to STM data away from the magic angles [43–45]. A natural choice of the reference point, which we adopt throughout this letter, is the CN point. This means that the single particle Hamiltonian $h_0(\mathbf{k})$ is given by

$$h_0(\mathbf{k}) = h_{\text{BM}}(\mathbf{k}) - h_{\text{HF}}(P_0, \mathbf{k}) \quad (7)$$

where $h_{\text{BM}}(\mathbf{k})$ is the BM Hamiltonian and P_0 is the projector corresponding to symmetry unbroken state obtained by filling the lower band of the BM Hamiltonian at CN. We note that in the different approach of Ref. [9] where multiple bands are included, the reference point was taken in the limit of decoupled layers. In our complementary approach of projection onto the flat bands it is not possible to implement such a choice.

Using CN as our reference point implies that the bands at empty or full filling should include some HF corrections leading to a modified band structure shown in Fig. 1 together with the resulting density of states (DOS). We notice that the separation between the two peaks in the DOS is about 10-15 meV in agreement with the measured DOS in STM experiments [43, 44, 46]. Thus, our approach provides an explanation for the discrepancy between the experimentally measured peak separation and the expectation based on the BM model whose bandwidth close to the magic angle is much smaller (1-3 meV).

III. SYMMETRY-BROKEN PHASES

The interacting TBG Hamiltonian is characterized by the following symmetries [4]: spinless time-reversal \mathcal{T} mapping the two valleys, $\text{SU}(2)$ spin rotation in each valley, $\text{U}(1)$ valley charge conservation and C_6 symmetry as well as a mirror symmetry which switches layers and sublattices but acts within each valley. Of these, only spin rotation, C_3 , mirror and $C_2\mathcal{T}$ act within each valley. At integer filling, different correlated insulating phases can emerge by breaking some of these symmetries. Time-reversal symmetry is broken by valley polarized (VP) states, where the filling of the two valleys is different. Spin rotation symmetry is broken by spin polarization (SP) leading to ferromagnetic order. $\text{U}(1)$ valley charge conservation is broken in the presence of intervalley coherent (IVC) superposition of states from the two valleys. C_2 symmetry is broken by sublattice polarization which gaps out the

Dirac points at the Moiré K and K' points.

Breaking C_3 symmetry alone does not generally lead to a gapped phase since it only moves the Dirac points away from the Moiré K and K' without gapping them out. Even strong C_3 breaking does not result in the merging and gapping of the Dirac nodes, in contrast with other familiar band structures such as single layer graphene. This follows from the fact that the chirality of the Dirac nodes, which is well defined in the presence of $C_2\mathcal{T}$ symmetry, is the equal [4, 15], rather than opposite. Alternately, one can phrase the argument as follows. The topology of the two flat bands is captured by the second Stiefel-Whitney invariant w_2 [41, 47, 48]. This invariant is protected by $C_2\mathcal{T}$ and only depends on the flat band eigenstates which are unaffected by any symmetry breaking that does not involve other bands (which is the main assumption in this work). Indeed, the w_2 invariant must be trivial for a single isolated band, implying we cannot separate the pair of connected flat bands [49]. Thus the non-trivial w_2 invariant implies that the two Dirac points cannot be removed without breaking $C_2\mathcal{T}$.

Before presenting the numerical results, let us make the following observations. First, it is relatively easy to show that a state with uniform full spin or valley polarization is always a self-consistent solution to the HF equations at CN for sufficiently narrow bands. These two states have the same energy in the absence of intervalley Hund’s coupling [17, 22]. The IVC state is known to have higher energy than SP/VP states for isolated bands with non-vanishing valley Chern number [17, 37]. These arguments do not generalize to TBG where the extra symmetries of the problem complicate the discussion (see Appendix and Ref. [50]). Nevertheless, we will exclude IVC orders from our numerical analysis (which is equivalent to assuming unbroken $\text{U}(1)$ valley charge conservation) since it leads to significant simplification by allowing us to focus on a single flavor (spin and valley). Different diagonal spin-valley orders can then be generated from the single-flavor solution by applying different symmetries. The energy competition with $\text{U}(1)$ valley symmetry broken phases is considered in [50].

IV. RESULTS

The results for the self-consistent HF analysis are provided in Fig. 2 showing the energies of the different solutions as a function of the C_3 symmetry breaking parameter β . There are two types of gapped solutions corresponding to either flavor-polarized (spin/valley) states or $C_2\mathcal{T}$ -breaking ($C_2\mathcal{I}$) insulators. There are three gapped solutions corresponding to spin-polarized (SP), valley-polarized (VP) and $C_2\mathcal{T}$ -breaking ($C_2\mathcal{I}$) insulators. The latter does not break C_3 when $\beta = 0$ but develops a large C_3 breaking component for $\beta \neq 0$. The extent of C_3 symmetry breaking can be quantified by defining

$$\chi_{C_3} = \frac{1}{N} \sum_{\mathbf{k}} (1 - |\langle \psi_{O_3\mathbf{k}} | C_3 | \psi_{\mathbf{k}} \rangle|^2), \quad (8)$$

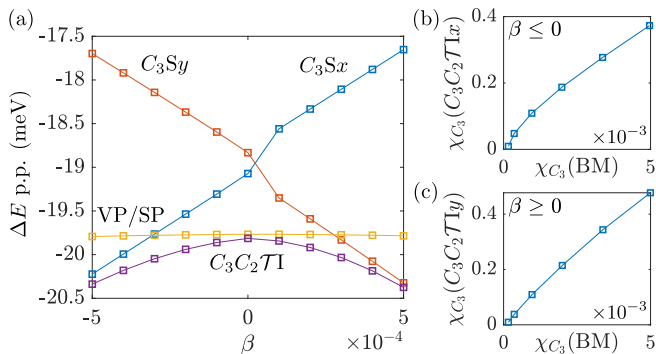


FIG. 2. (a) Energies of the solutions of the self-consistent HF equations as a function of the C_3 symmetry breaking parameter β . All energies are measured relative to the state with no-broken symmetry. The degree of C_3 -breaking measured by χ_{C_3} (Eq. 8) for the $C_2\mathcal{T}$ -breaking insulator as a function χ_{C_3} for the non-interacting system for $0 \leq |\beta| \leq 5 \times 10^{-4}$ are shown in panels (b) and (c) for positive and negative values of β , respectively.

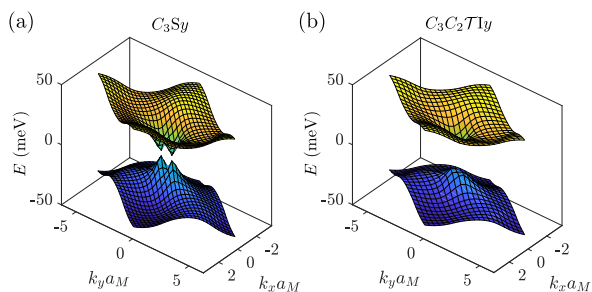


FIG. 3. 3D band structure for one of the (a) C_3 -breaking semimetals and (b) $C_2\mathcal{T}$ breaking valley Hall insulators.

which vanishes for any C_3 -symmetric state. Here, $|\psi_{\mathbf{k}}\rangle$ are the occupied single-particle eigenstates of the HF Hamiltonian with momentum \mathbf{k} (for a given flavor). The value of χ_{C_3} for the $C_2\mathcal{T}I$ state is shown in Fig. 2 as a function of χ_{C_3} for the corresponding non-interacting states arising from explicit C_3 -breaking parameter $\beta \neq 0$ in the BM model. We can clearly see from the figure that a relatively small $\chi_{C_3}(BM) \sim 10^{-3}$ in the non-interacting states induces a much larger C_3 symmetry breaking of almost two orders of magnitude in the $C_2\mathcal{T}I$ state. This serves to show that the $C_2\mathcal{T}I$ has very large susceptibility to C_3 symmetry breaking. In the following, we will refer to this state for positive and negative β as C_3C_2Tly and C_3C_2Tlx , respectively. In addition to this insulating state, there are two distinct C_2 -preserving semimetallic phases which spontaneously break C_3 even for $\beta = 0$ which we denote by C_3Sx and C_3Sy , since they have Dirac points along k_x and k_y , respectively. We notice that these ground states are similar to the ones obtained within a 10-band model Ref. [43] which used a site-local ansatz for the interactions. Examples of the band structures for the C_3Sy and C_3C_2Tly states are shown in Fig. 3.

The $C_2\mathcal{T}I$ phase obtained here is characterized by a Chern number of ± 1 for a given spin and valley. The nature of the resulting phase depends on the precise symmetries which are

broken as follows: (i) if \mathcal{T} is broken but C_2 and spin rotation are preserved, we obtain a quantum anomalous Hall (QAH) insulator with total Chern number $C = \pm 4$, (ii) if spin rotation is broken we obtain a quantum-spin Hall (QSH) insulator with opposite Chern number $C_s = \pm 2$ for opposite spins, (iii) if C_2 is broken but \mathcal{T} and spin rotation symmetry are preserved, then a quantum valley Hall (QVH) insulator obtains with opposite Chern number $C_v = \pm 2$ for opposite valleys, or (iv) we can additionally break spin rotation symmetry to obtain a state where opposite spins within the same valley also have opposite Chern numbers resulting in a quantum spin-valley Hall (QSVH) insulator where flipping either spin or valley flips the Chern number. There can also be states with total Chern number ± 2 , but these do not lead to any new physics or a lower energy, therefore we restrict to the above four possibilities for simplicity. The QH, QSH and QVSH preserve either C_2 or a combination of C_2 and some internal symmetries, thus the only state expected to couple to the C_2 -breaking hBN substrate is the QVH which is likely to be energetically favored in aligned samples[51]. The energies of the four possible $C_2\mathcal{T}$ states are very similar differing only by very small $\sim 10^{-3}$ meV Hartree corrections. Similarly, the flavor-polarized state can be spin-polarized, breaking $SU(2)$ spin rotation, valley-polarized breaking \mathcal{T} or a spin-valley-locked states which breaks both but preserves a combination of \mathcal{T} and π -spin rotation. These states are degenerate on the mean field level and are only distinguished by intervalley Hund's coupling [17, 22] neglected in this study.

At $\beta = 0$, the energies of the insulating VP/SP and $C_2\mathcal{T}I$ states are very close and smaller by about 1 meV per particle than the energies of the two semimetallic C_3 breaking states. An explanation for this fact is provided in the next section in the limit where the intrasublattice hopping is switched off [52]. In this limit, we can establish a rigorous bound for the Fock energy which plays the dominant role in the energy competition. We will show that the SP/VP and the $C_2\mathcal{T}I$ states saturate the bound in this limit and should thus be approximately degenerate. The energies of the C_3S states are higher than these two. This analysis explains why these states are expected to be close in energy, but it is generally insufficient to capture the details of the energy competition which depends sensitively on the intrasublattice hopping w_0 and can only be determined numerically. A more detailed analysis of the effects of dispersion and finite sublattice symmetry breaking w_0 is given in Ref. [50].

Once β becomes non-zero, the energy of the $C_2\mathcal{T}$ breaking state is reduced relative to the VP/SP state. Furthermore, one of the two C_3 -breaking states (depending on the sign of β) goes down in energy becoming more energetically favorable to the VP/SP state around $\beta = \pm 3 \times 10^{-4}$. For larger values of $\beta \gtrsim 4 \times 10^{-4}$, the energies of the insulating $C_2\mathcal{T}$ -breaking phase and the semimetallic $C_2\mathcal{T}$ -preserving phase approach the same value. This indicates that even very small explicit C_3 -breaking picks out these two states as the main candidates for the ground state at CN. Assuming that such small explicit C_3 symmetry breaking exists in real samples due to strain, our analysis leads to the conclusion that the ground state of TBG at CN is either a $C_2\mathcal{T}$ -breaking insulator or a $C_2\mathcal{T}$ -symmetric

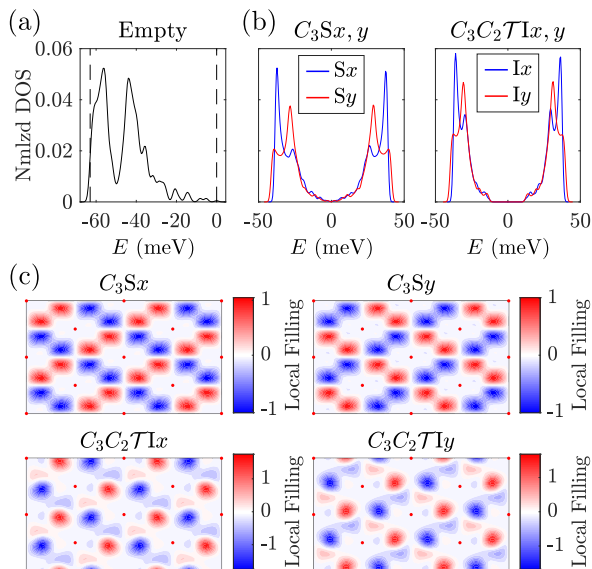


FIG. 4. (a) Normalized DOS of the empty filling band structure. The two vertical dashed lines indicate the band bottom and top which is chosen to be at $E = 0$. (b) Normalized DOS and (c) local filling fraction for the upper layer defined in (24) for the four potential ground states for strain parameter $\beta = \pm 4 \times 10^{-4}$. For positive (negative) beta: the two competing ground states are a $C_2\mathcal{T}$ -preserving semimetal C_3S_y (C_3S_x) and a $C_2\mathcal{T}$ -breaking valley Hall insulator $C_3C_2\mathcal{T}I_y$ ($C_3C_2\mathcal{T}I_x$), both strongly breaking C_3 . The red dots in (c) indicates the AA position. In (c) the breaking of C_2 and C_3 rotation symmetries are clearly visible.

semimetal. Both states strongly break C_3 symmetry and are very close in energy. It is worth noting that, in the presence of disorder, massless Dirac fermions may also emerge from the spatial domain walls of locally $C_2\mathcal{T}$ breaking insulating regions [53].

V. ENERGY COMPETITION IN CHIRAL LIMIT

The existence of several states close in energy can be explained by considering the simplified chiral model of Ref. [52] where the Moiré intrasublattice hopping is switched off. In such limit, the band becomes strictly flat at charge neutrality in the absence of interaction and the model has an extra sublattice symmetry i.e. the single-particle Hamiltonian anticommutes with the sublattice operator σ_z . As a result, the flatband wavefunctions can be chosen to be eigenfunctions of σ_z such that the wavefunction $\sigma_z u_{A/B, \tau, \mathbf{k}} = \pm u_{A/B, \tau, \mathbf{k}}$. In this limit, we can show (see Appendix for details) that the form factor matrix has the simple form

$$\Lambda_{\mathbf{q}}(\mathbf{k}) = F_{\mathbf{q}}(\mathbf{k}) e^{i\Phi_{\mathbf{q}}(\mathbf{k})\sigma_z\tau_z}, \quad (9)$$

where $F_{\mathbf{q}}(\mathbf{k})$ and $\Phi_{\mathbf{q}}(\mathbf{k})$ denoting the magnitude and phase of the form factor for the flatband wavefunction in sublattice A and valley K.

Let us now compare the mean field energy for different

phases. First, we notice that, even in the chiral limit where the non-interacting band dispersion vanishes, a sizable dispersion would be generated by the interaction [50]. It will be instructive, however, to start by ignoring the interaction generated band dispersion and focusing on the Hartree-Fock energy. At a fixed integer filling, the Hartree term does not play a role in the energy competition between phases so we can focus on the Fock term. We will find it convenient to write the projector $P(\mathbf{k})$ as

$$P(\mathbf{k}) = \frac{1}{2}[1 + Q(\mathbf{k})], \quad Q(\mathbf{k})^2 = 1, \quad \text{tr} Q(\mathbf{k}) = 0 \quad (10)$$

In terms of Q , the Fock energy is given by

$$E_F = -\frac{1}{8A} \sum_{\mathbf{k}, \mathbf{q}} V_{\mathbf{q}} \text{tr} Q(\mathbf{k}) \Lambda_{\mathbf{q}}^\dagger(\mathbf{k}) Q(\mathbf{k} + \mathbf{q}) \Lambda_{\mathbf{q}}(\mathbf{k}). \quad (11)$$

up to a constant. We note that $\langle A, B \rangle = \text{tr} AB$ defines a positive definite inner product on the space of hermitian matrices. Using Cauchy-Schwarz inequality, we get

$$E_F \geq E_{F, \min} = -\frac{1}{A} \sum_{\mathbf{k}, \mathbf{q}} V_{\mathbf{q}} F_{\mathbf{q}}^2(\mathbf{k}). \quad (12)$$

This inequality is satisfied if and only if $Q(\mathbf{k} + \mathbf{q})$ is parallel to $\Lambda_{\mathbf{q}}(\mathbf{k}) Q(\mathbf{k}) \Lambda_{\mathbf{q}}^\dagger(\mathbf{k})$ for every \mathbf{k} and \mathbf{q} which implies

$$Q(\mathbf{k} + \mathbf{q}) = e^{i\Phi_{\mathbf{q}}(\mathbf{k})\sigma_z\tau_z} Q(\mathbf{k}) e^{-i\Phi_{\mathbf{q}}(\mathbf{k})\sigma_z\tau_z}, \quad (13)$$

A \mathbf{k} -independent flavor (spin, valley) polarized state obviously satisfies this constraint since $\sigma_z\tau_z$ is diagonal in flavor, thereby saturating the Fock bound. This state can either be spin-polarized $Q = s_z$, valley polarized $Q = \tau_z$ or spin-valley locked $Q = \tau_z s_z$.

Next let us discuss $C_2\mathcal{T}$ breaking insulating solutions. A $C_2\mathcal{T}$ breaking solution to Eq. 13 is obtained by taking $Q_{\mathbf{k}} = \sigma_z$ (since $C_2\mathcal{T}$ is off diagonal in the sublattice index). The resulting state saturates the Fock bound and is characterized by a Chern number ± 1 in the lower band. Its energy competition with the flavor-polarized states is settled by the effects of the single-particle term $h_{\mathbf{k}}$ and w_0 which are neglected here. In our numerics, we found that these states are very close in energy for the realistic model with their energy difference only sensitive to the strain parameter β . Depending on its structure in flavor space, the $C_2\mathcal{T}$ -breaking insulator may correspond to one of four states: (i) $Q = s_0\tau_0\sigma_z$ breaks C_2 but not \mathcal{T} and corresponds to a valley Hall state, (ii) $Q = s_0\tau_z\sigma_z$ breaks \mathcal{T} but not C_2 and corresponds to a quantum Hall state with Chern number ± 4 , (iii) $Q = s_z\tau_0\sigma_z$ corresponds to a valley-spin-Hall state where the Chern number is invariant under flipping spin and valley, and (iv) $Q = s_z\tau_z\sigma_z$ corresponds to a spin-Hall state.

Finally, let us consider semimetallic states which break neither flavor nor $C_2\mathcal{T}$ symmetry. These can be generally described (within each flavor) by the order parameter

$$Q_{\text{SM}}(\mathbf{k}) = \sigma_x e^{i\alpha_{\mathbf{k}}\sigma_z\tau_z}. \quad (14)$$

Substituting in the Fock energy (11) yields

$$E_F = -\frac{1}{A} \sum_{\mathbf{k}, \mathbf{q}} V_{\mathbf{q}} F_{\mathbf{q}}^2(\mathbf{k}) \cos[\alpha_{\mathbf{k}} - \alpha_{\mathbf{k}+\mathbf{q}} + 2\Phi_{\mathbf{q}}(\mathbf{k})]. \quad (15)$$

To simplify further, we make the reasonable assumption that $F_{\mathbf{q}}(\mathbf{k})$ decays quickly with the relative momentum \mathbf{q} which enables us to expand $\Phi_{\mathbf{q}}(\mathbf{k})$ and $\alpha_{\mathbf{k}+\mathbf{q}}$ in \mathbf{q} . Noting that $\Phi_{\mathbf{q}}(\mathbf{k}) = \mathbf{q} \cdot \mathbf{A}_{\mathbf{k}} + O(q^2)$ with $\mathbf{A}_{\mathbf{k}}$ the Berry connection $-i\langle u_{A,K,\mathbf{k}} | \nabla_{\mathbf{k}} | u_{A,K,\mathbf{k}} \rangle$, we get

$$E_F = E_{F,\min} + \frac{1}{2A} \sum_{\mathbf{k}, \mathbf{q}} V_{\mathbf{q}} q^2 F_{\mathbf{q}}^2(\mathbf{k}) (\nabla_{\mathbf{k}} \alpha_{\mathbf{k}} - 2\mathbf{A}_{\mathbf{k}})^2. \quad (16)$$

The second term in the energy is non-negative and implies that the semimetal does not generally satisfy the bound. In fact, this term has the form of the energy of a superconductor in a magnetic field in momentum space. Due to the non-trivial Chern number of the sublattice-polarized bands [50, 52], the Bloch wavefunctions cannot be chosen to be simultaneously smooth and periodic over the Brillouin zone. If we choose them to be smooth, the Berry connection $\mathbf{A}_{\mathbf{k}}$ will be smooth but the phase $\alpha_{\mathbf{k}}$ will necessarily wind by 4π around the Brillouin zone, leading to at least two vortices in the Brillouin zone where the projector is undefined due to the vanishing of the gap. These will yield a finite contribution to the second term which implies that the semimetal never satisfies the Fock bound in the ideal limit [54]. The location of the vortices which minimize this term is determined by the competition between the weak (logarithmic) repulsion between the vortices in 2D and the tendency of the vortices to sit wherever the magnetic field corresponding to \mathbf{A} , i.e. the Berry curvature, is maximal. As shown in Fig. 5, in the chiral limit $w_0 = 0$, the Berry curvature is relatively uniform so that vortices prefer to sit far apart at the K and K' point, thereby preserving C_3 symmetry. However, for finite w_0/w_1 , the Berry curvature (in the basis which diagonalizes the sublattice operator σ_z [50]) becomes strongly peaked at the Γ point and for the realistic parameter $w_0/w_1 \approx 0.75$, the vortices prefer to sit close to the Γ point. This explains the energetic advantage of C_3 symmetry breaking in the realistic parameter regime considered in the numerics.

Finally, let us consider the effect of the dispersion (which is mostly generated by the interaction). Using $C_2\mathcal{T}$, valley and particle-hole symmetries, the form of the dispersion can be reduced to [50]

$$h_0(\mathbf{k}) = \sigma_x f(\mathbf{k}) e^{i\phi(\mathbf{k})\sigma_z\tau_z} \quad (17)$$

where $f(\mathbf{k})$ is a positive real function which vanishes at the two Dirac points and $\phi(\mathbf{k})$ winds by 2π around each of the Dirac points. These points lie at the Moiré K_M and K'_M for $\beta = 0$ but move away for finite β . The energy contribution of $h_0(\mathbf{k})$ for a state described by the matrix Q is

$$E_h[Q] = \frac{1}{2} \sum_{\mathbf{k}} \text{tr} h_0(\mathbf{k}) Q(\mathbf{k}) \quad (18)$$

We notice that this term favors the semimetal order parameter with Q given by (14) but vanishes for all the order parameters which satisfy the Fock bound. This might suggest none of these states benefit energetically from dispersion but this turns out not to be true as we will show below.

We start by writing the total energy functional in terms of Q (ignoring the Hartree term which does not play a role in the competition between phases)

$$E[Q] = E_h[Q] + E_F[Q] \quad (19)$$

with $E_h[Q]$ given by (18) and $E_F[Q]$ given by (11). The Hartree-Fock self consistency equation is taken by setting the variation of $E[Q]$ relative to Q to zero (subject to the constraint $Q^2 = 1$) which leads to the equation

$$[Q(\mathbf{k}), \frac{1}{2}h_0(\mathbf{k}) - \frac{1}{4A} \sum_{\mathbf{q}} V_{\mathbf{q}}(\mathbf{k}) \Lambda_{\mathbf{q}}(\mathbf{k})^* Q(\mathbf{k}+\mathbf{q}) \Lambda_{\mathbf{q}}(\mathbf{k})^T] = 0 \quad (20)$$

From this equation, we see that the flavor polarized states which are characterized by $[Q, h_0] = 0$ remain solution of the self-consistency equation for non-zero h_0 whereas the $C_2\mathcal{T}$ breaking insulators which are characterized by $\{Q, h_0\} = 0$ are no longer solution to the self-consistency equation. To write a $C_2\mathcal{T}$ breaking solution, we write

$$Q(\mathbf{k}) = Q_{C_2\mathcal{T}}(\mathbf{k}) \cos \theta(\mathbf{k}) + Q_{\text{SM}}(\mathbf{k}) \sin \theta(\mathbf{k}) \quad (21)$$

which satisfies the condition $Q^2 = 1$ due to the anticommutation of $Q_{C_2\mathcal{T}}$ and Q_{SM} . The \mathbf{k} dependence of θ can be determined from the self-consistency condition (20). In the following, we will assume for simplicity that θ is \mathbf{k} independent and choose it to minimize the the total energy (19) leading to

$$|\sin \theta| = \frac{E_h[Q_{\text{SM}}]}{2(E_F[Q_{\text{SM}}] - E_{F,\min})} \quad (22)$$

where we used the fact that $Q_{C_2\mathcal{T}}$ saturates the Fock bound. We notice that the denominator is the same as the second term on the right hand side of (16) which is guaranteed to be finite and roughly of the order of the interaction scale. This implies that θ is small whenever the interaction dominates the dispersion. In this case, the order parameter described by (21) is very close to the pure insulator order parameter. The corresponding energy is given by

$$E[Q] = E_{F,\min} - \frac{E_h[Q_{\text{SM}}]^2}{4(E_F[Q_{\text{SM}}] - E_{F,\min})} \quad (23)$$

Thus, the $C_2\mathcal{T}$ -breaking insulators actually benefit from the dispersion in quadratic order by developing a small component proportional to the semimetal order parameter. This explains why their energy is decreased in response to explicit C_3 -breaking which energetically favors the semimetal (thus increasing $|E_h[Q_{\text{SM}}]|$). It also explains their high C_3 -breaking susceptibility which mainly arises from their Q_{SM} component.

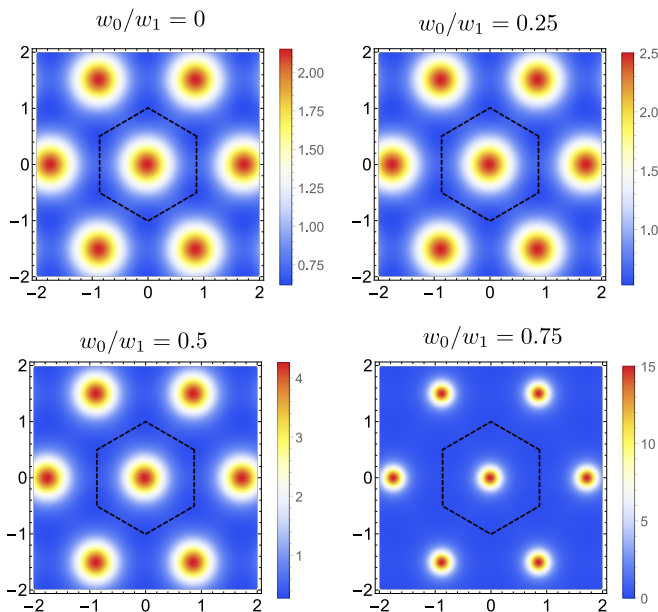


FIG. 5. Berry curvature in the sublattice polarized basis for different values of the ratio w_0/w_1 .

VI. CONSEQUENCES FOR EXPERIMENT

The possibility of C_3 breaking at CN is consistent with several recent reports [43–46] which observed direct evidence of C_3 breaking in STM measurements. To check the compatibility of these measurements with our mean-field solutions, we compute the DOS for the four possible C_3 -breaking states (arising for positive or negative values of β) in Fig. 4b. We see that in all cases the global DOS consists of two broad peaks (which are sometimes further split into two) separated by about 60–80 meV, in agreement with the STM measurements [43, 45]. The DOS alone however, is insufficient to distinguish the insulating and semi-metallic state, since both have very low DOS close to zero energy. One way to distinguish the two is to compute the local filling fraction defined as [44]

$$\nu(\mathbf{r}) = 8 \left(\frac{\rho_{\text{LB}}(\mathbf{r})}{\rho_{\text{LB}}(\mathbf{r}) + \rho_{\text{UB}}(\mathbf{r})} - \frac{1}{2} \right) \in [-4, 4], \quad (24)$$

where $\rho_{\text{LB/UB}}(\mathbf{r})$ denote the integrated local DOS from the upper layer for the lower/upper band. $\nu(\mathbf{r})$, shown in Fig. 4, exhibits clear C_3 -symmetry breaking pattern for all the four

phases. The patterns for the $C_3\text{S}$ and $C_3C_2\text{TI}$ QVH phases can be distinguished by C_2 symmetry which is visibly present in the former but absent in the latter (the pattern of the other $C_3C_2\text{TI}$ is obtained by symmetrizing the QVH result relative to C_2 with the result being very similar to the one for the $C_3\text{S}$ breaking states up to an overall factor). The $C_3\text{S}$ pattern is qualitatively similar to that measured in Ref. [44], with the density vanishing at the Kagomé lattice site lying on the mirror plane and changing sign twice around it, while having non-vanishing magnitude with opposite signs on the other two Kagomé lattice sites. Such structure is generic for any C_3 -breaking phase which preserves mirror and particle-hole symmetries [55] and a combination of C_2 and some local symmetry. [56]

VII. CONCLUSION

In conclusion, we have performed a momentum-space self-consistent Hartree-Fock analysis to uncover the nature of the symmetry-broken phase in twisted bilayer graphene at charge neutrality. In addition to insulating states corresponding to spin, valley or sublattice polarization, we found two C_3 -breaking $C_2\mathcal{T}$ -symmetric semimetallic solutions. Our main finding is that the existence of very small explicit C_3 -breaking energetically favors one of these $C_2\mathcal{T}$ -symmetric metallic state together with $C_2\mathcal{T}$ -breaking insulating states. Both sets of states have similar energy within HF, strongly break C_3 symmetry and are consistent with the density of states measured in STM experiments. They can be experimentally distinguished in transport measurements or by comparing space-resolved local filling fractions in STM. We propose these two states as candidates for the insulating and conducting states observed in different experiments at the CNP and suggest that the competition between the two is settled by small details that are likely sample-dependent.

ACKNOWLEDGMENTS

We thank Eva Andrei, Allan MacDonald, Adrian Po, A. Thomson and M. Xie for helpful discussions. S. L., E. K., J. Y. L. and A. V. were supported by a Simons Investigator Fellowship and by NSF-DMR 1411343. E. K. was supported by the German National Academy of Sciences Leopoldina through grant LPDS 2018-02 Leopoldina fellowship.

Appendix A: Single-particle physics: Bistritzer-Macdonald model

Our starting point is the Bistritzer-MacDonald (BM) model of the TBG band structure [32], which we now briefly review. We begin with two layers of perfectly aligned (AA stacking) graphene sheets extended along the xy plane, and we choose the frame orientation such that the y -axis is parallel to some of the honeycomb lattice bonds. Now we choose an arbitrary atomic site and twist the top and bottom layers around that site by the counterclockwise angles $\theta/2$ and $-\theta/2$ (say $\theta > 0$), respectively. When θ is very small, the lattice form a Moiré pattern with very large translation vectors; correspondingly, the Moiré Brillouin zone

(MBZ) is very small compared to the monolayer graphene Brillouin zone (BZ), as illustrated in Fig. 6. In this case, coupling between the two valleys can be neglected. If we focus on one of the two valleys, say K , then the effective Hamiltonian is given by:

$$\mathcal{H}_+ = \sum_l \sum_{\mathbf{k}} \tilde{f}_l^\dagger(\mathbf{k}) h_{\mathbf{k}}(l\theta/2) \tilde{f}_l(\mathbf{k}) + \left(\sum_{\mathbf{k}} \sum_{i=1}^3 \tilde{f}_i^\dagger(\mathbf{k} + \mathbf{q}_i) T_i \tilde{f}_b(\mathbf{k}) + h.c. \right). \quad (\text{A1})$$

Here, $l = t/b \simeq \pm 1$ is the layer index, and $\tilde{f}_l(\mathbf{k})$ is the K -valley electron originated from layer l . The sublattice index σ is suppressed, thus each $\tilde{f}_l(\mathbf{k})$ operator is in fact a two-component column vector. $h_{\mathbf{k}}(\theta)$ is the monolayer graphene K -valley Hamiltonian with twist angle θ :

$$h_{\mathbf{k}}(\theta) = \hbar v_F \begin{pmatrix} 0 & (k_x - ik_y)e^{i\theta} \\ (k_x + ik_y)e^{-i\theta} & 0 \end{pmatrix}, \quad (\text{A2})$$

where $v_F = 9.1 \times 10^5$ m/s is the Fermi velocity. Let K_l be the K -vector of layer l , then \mathbf{q}_1 is defined as $K_b - K_t$. $\mathbf{q}_2 = O_3 \mathbf{q}_1$ is the counterclockwise 120° rotation of \mathbf{q}_1 , and $\mathbf{q}_3 = O_3 \mathbf{q}_2$. Finally, the three matrices T_i are given by

$$T_1 = (1 + \beta) \begin{pmatrix} w_0 & w_1 \\ w_1 & w_0 \end{pmatrix}, \quad T_2 = \begin{pmatrix} w_0 & w_1 e^{-2\pi i/3} \\ w_1 e^{2\pi i/3} & w_0 \end{pmatrix}, \quad T_3 = \begin{pmatrix} w_0 & w_1 e^{2\pi i/3} \\ w_1 e^{-2\pi i/3} & w_0 \end{pmatrix}, \quad (\text{A3})$$

where we introduced an explicit C_3 -breaking parameter β . We take $w_1 = 110$ meV and $w_0 = 82.5$ meV. The difference between w_0 and w_1 reflects the effect of lattice relaxation. Note that the argument of $\tilde{f}_l(\mathbf{k})$ is measured from K_l , i.e. the monolayer UV momentum associated to $\tilde{f}_l(\mathbf{k})$ is in fact $K_l + \mathbf{k}$. It is convenient to also choose a common momentum reference point for the two layers. For example, we can define $f_t(\mathbf{k}) = \tilde{f}_t(\mathbf{k} - \mathbf{q}_3)$ and $f_b(\mathbf{k}) = \tilde{f}_b(\mathbf{k} + \mathbf{q}_2)$, such that the arguments for both f_t and f_b are measured from $K_t - \mathbf{q}_3$, indicated as γ in the right panel of Fig. 6.

One intuitive way of thinking about this effective Hamiltonian is to imagine a honeycomb lattice of Dirac points in the momentum space, as shown in Fig. 7b, where the two sublattices correspond to the two layers. A Dirac point at momentum \mathbf{q} contributes a diagonal block $h_{\mathbf{k}-\mathbf{q}}(\pm\theta/2)$ to the Hamiltonian for the MBZ momentum \mathbf{k} , where the sign is determined by the sublattice that \mathbf{q} belongs to. The off-diagonal blocks T_i are nothing but the nearest-neighbor couplings of these Dirac points.

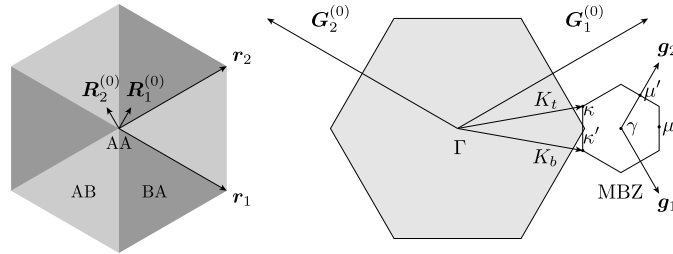


FIG. 6. Real space (left) and momentum space (right) structures for both monolayer and Moiré lattices of twisted bilayer graphene. In the real space (left) panel, we also show the underlying Moiré pattern structure.

When the twist angle is near the magic angle $\theta = 1.05^\circ$, two isolated flat bands per spin and valley appear near the charge neutrality (CN) Fermi energy, shown in Fig. 7a. These two bands are the focus of the current work.

The single particle Hamiltonian within each valley \mathcal{H}_\pm is invariant under the following symmetries

$$C_3 \tilde{f}_{\mathbf{k}} C_3^{-1} = e^{-\frac{2\pi}{3} i \tau_z \sigma_z} \tilde{f}_{C_3 \mathbf{k}}, \quad (C_2 \mathcal{T}) \tilde{f}_{\mathbf{k}} (C_2 \mathcal{T})^{-1} = \sigma_x \tilde{f}_{\mathbf{k}}, \quad \mathcal{M}_y \tilde{f}_{\mathbf{k}} \mathcal{M}_y^{-1} = \sigma_x \mu_x \tilde{f}_{M_y \mathbf{k}}, \quad (\text{A4})$$

In addition, the two valleys are related by time-reversal symmetry given by

$$\mathcal{T} \tilde{f}_{\mathbf{k}} \mathcal{T}^{-1} = \tau_x \tilde{f}_{-\mathbf{k}}. \quad (\text{A5})$$

Here, σ , τ and μ denote the Pauli matrices in sublattice, valley and layer spaces, respectively.

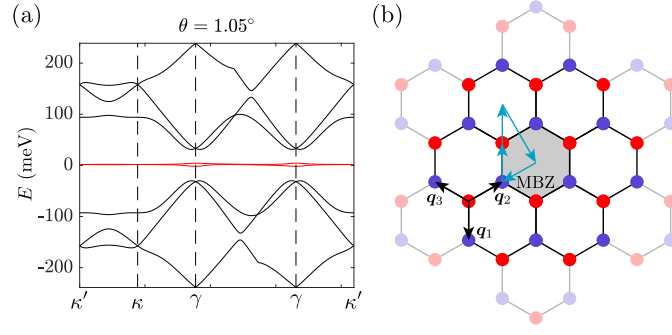


FIG. 7. (a) Band structure of magic-angle TBG obtained from the BM model. The sampling path is shown by the cyan arrows in the right panel. (b) Dirac point lattice at the MBZ.

Appendix B: Projecting the interaction onto the flat bands

In the following, we derive the form of the interaction when projecting onto the two flat bands. Since these two bands have a Wannier obstruction, we can only write such projected interaction in k -space. Let $c_{\alpha}^{\dagger}(\mathbf{k})$ be the creation operator for the energy eigenstate in the band structure with internal flavor μ and band index n , where $\mu = (\tau, s)$ is a collective index including both valley $\tau = \pm$ and spin $s = \uparrow / \downarrow$, and $n = 1, 2$ represents the lower and upper bands, respectively. Also let $f_{\mu, I}^{\dagger}(\mathbf{q})$ be the “elementary” continuous fermion with monolayer momentum \mathbf{q} , flavor $\mu = (\tau, s)$ and $I = (l, \sigma)$ representing layer and sublattice, then c^{\dagger} and f^{\dagger} are related to each other by the k -space wave functions as follows:

$$c_{\mu, n}^{\dagger}(\mathbf{k}) = \sum_{\mathbf{G}, I} u_{\tau, n; \mathbf{G}, I}(\mathbf{k}) f_{\mu, I}^{\dagger}(\mathbf{k} + \mathbf{G}), \quad (\text{B1})$$

where \mathbf{G} is a Moiré reciprocal lattice vector. In the above expression, we are already using the fact that the wave functions are spin-independent. Once we choose a gauge of $u_{\tau, n; \mathbf{G}, I}(\mathbf{k})$ for all \mathbf{k} in some MBZ, $c^{\dagger}(\mathbf{k})$ are defined in terms of the $f^{\dagger}(\mathbf{q})$ for those \mathbf{k} , and whenever necessary, we define $c^{\dagger}(\mathbf{k} + \mathbf{G}) = c^{\dagger}(\mathbf{k})$ for any reciprocal lattice vector \mathbf{G} , which is equivalent to defining $u_{\tau, n; \mathbf{G}, I}(\mathbf{k} + \mathbf{G}_0) = u_{\tau, n; \mathbf{G} + \mathbf{G}_0, I}(\mathbf{k})$. Note that the momentum argument for f^{\dagger} is unconstrained since we are using the continuum theory for monolayers of graphene. We choose the normalization $\{f_{\mu, I}(\mathbf{q}), f_{\mu', I'}^{\dagger}(\mathbf{q}')\} = \delta_{\mu\mu'} \delta_{II'} \delta_{\mathbf{q}\mathbf{q}'}$ (suppose the system size is finite), and $\langle u_{\tau, n}(\mathbf{k}) | u_{\tau', n'}(\mathbf{k}) \rangle := \sum_{\mathbf{G}, I} u_{\tau, n; \mathbf{G}, I}^*(\mathbf{k}) u_{\tau', n'; \mathbf{G}, I}(\mathbf{k}) = \delta_{\tau\tau'} \delta_{nn'}$, which imply $\{c_{\mu, n}(\mathbf{k}), c_{\mu', n'}^{\dagger}(\mathbf{k}')\} = \delta_{\mu\mu'} \delta_{nn'} \delta_{\mathbf{k}\mathbf{k}'}$ when \mathbf{k}, \mathbf{k}' are confined in the MBZ. For the purpose of projecting the interaction into these two bands, it is convenient to introduce the form factor notation:

$$\lambda_{mn, \tau; \mathbf{q}}(\mathbf{k}) := \langle u_{\tau, m}(\mathbf{k}) | u_{\tau, n}(\mathbf{k} + \mathbf{q}) \rangle \quad (\text{B2})$$

where \mathbf{q} is not restricted to the first Brillouin zone. The form factors satisfy

$$\lambda_{mn, \tau; \mathbf{q}}(\mathbf{k}) = \lambda_{nm, \tau; -\mathbf{q}}(\mathbf{k} + \mathbf{q})^* \quad (\text{B3})$$

just from the definition, and also has the property

$$\lambda_{mn, \tau; \mathbf{q}}(\mathbf{k}) = \lambda_{mn, -\tau; -\mathbf{q}}(-\mathbf{k})^* \quad (\text{B4})$$

due to the time-reversal symmetry.

The interaction Hamiltonian is given by

$$\mathcal{H}_{\text{int}} = \frac{1}{2A} \sum_{\sigma, \sigma', \tau, \tau'} \sum_{\mathbf{q}} V(\mathbf{q}) : \rho_{\sigma, \tau, \mathbf{q}} \rho_{\sigma', \tau', -\mathbf{q}} :, \quad (\text{B5})$$

where A is the total area of the system and $V(\mathbf{q})$ is the momentum space interaction potential, related to the real-space one by

$V(\mathbf{q}) := \int d^2\mathbf{r} V(\mathbf{r}) e^{-i\mathbf{q}\cdot\mathbf{r}}$. Depending on the number of gates, $V(\mathbf{q})$ takes the following form in the SI units:

$$V(\mathbf{q}) = \frac{e^2}{2\epsilon\epsilon_0 q} \begin{cases} (1 - e^{-2qd_s}), & \text{(single-gate)} \\ \tanh(qd_s), & \text{(dual-gate)} \end{cases} \quad (\text{B6})$$

where the screening length d_s is nothing but the distance from the graphene plane to the gate(s). Projecting onto the two narrow bands, this Hamiltonian has the form

$$\mathcal{H}_{\text{int}} = \frac{1}{2A} \sum_{\sigma, \sigma', \tau, \tau'} \sum_{\mathbf{q}, n_1, n_2, n_3, n_4} \sum_{\mathbf{k}_1, \mathbf{k}_2 \in \text{BZ}} \lambda_{n_1, n_2; \tau, \mathbf{q}}(\mathbf{k}_1) V(\mathbf{q}) \lambda_{n_4, n_3; \tau', \mathbf{q}}^*(\mathbf{k}_2) \\ \times c_{n_1, \sigma, \tau}^\dagger(\mathbf{k}_1) c_{n_3, \sigma', \tau'}^\dagger(\mathbf{k}_2 + \mathbf{q}) c_{n_4, \sigma', \tau'}(\mathbf{k}_2) c_{n_2, \sigma, \tau}(\mathbf{k}_1 + \mathbf{q}). \quad (\text{B7})$$

Appendix C: Hartree-Fock analysis in the chiral limit

The chiral limit of the BM model is obtained by switching off the w_0 term in (A3) [52]. In this limit, the bands become exactly flat at the magic angle and the eigenstates of the Hamiltonian have a simple form similar to the Landau levels on a torus. In the chiral limit, the single particle Hamiltonian anticommutes with the chiral (sublattice) symmetry operator given by $\Gamma = \sigma_z$. In addition, it is invariant under the particle-hole symmetry $\mathcal{P} \hat{f}_{\mathbf{k}} \mathcal{P}^{-1} = i\sigma_x \mu_y \hat{f}_{-\mathbf{k}}^\dagger$ (modulo a small basis rotation gauging away the θ dependence). This means that we can choose the wavefunctions for the flat bands to be eigenfunctions of the sublattice operator σ_z i.e. completely sublattice polarized [50]. The wavefunctions can then be labelled by their sublattice index $\sigma = A/B$. This means that the sublattice off-diagonal components of the form factor vanishes, i.e. $\lambda_{AB; \tau, \mathbf{G}}(\mathbf{k}, \mathbf{k}') = \lambda_{BA; \tau, \mathbf{G}}(\mathbf{k}, \mathbf{k}') = 0$. Furthermore, the action of $C_2\mathcal{T}$ is given by

$$C_2\mathcal{T}u_{A, \tau, \mathbf{k}} = e^{i\phi_{A, \tau, \mathbf{k}}} u_{B, \tau, \mathbf{k}}^*, \quad C_2\mathcal{T}u_{B, \tau, \mathbf{k}} = e^{i\phi_{B, \tau, \mathbf{k}}} u_{A, \tau, \mathbf{k}}^* \quad (\text{C1})$$

which implies that $\lambda_{AA; \tau, \mathbf{q}}(\mathbf{k}) = \lambda_{BB; \tau, \mathbf{q}}(\mathbf{k})^*$. Finally, we can use \mathcal{PT} symmetry to restrict the form factors further by noting that it exchanges positive and negative energy eigenstates in opposite valleys and sublattices

$$\mathcal{PT}u_{A, \tau, \mathbf{k}} = e^{i\eta_{A, \tau, \mathbf{k}}} u_{B, -\tau, \mathbf{k}}, \quad \mathcal{PT}u_{B, \tau, \mathbf{k}} = e^{-i\eta_{B, \tau, \mathbf{k}}} u_{A, -\tau, \mathbf{k}} \quad (\text{C2})$$

which implies that $\lambda_{A/B, \tau, \mathbf{q}}(\mathbf{k}) = \lambda_{B/A, -\tau, \mathbf{q}}(\mathbf{k})$. Summarizing these conditions, we can write

$$\lambda_{\sigma\sigma'; \tau, \mathbf{q}}(\mathbf{k}) = \delta_{\sigma\sigma'} F_{\mathbf{q}}(\mathbf{k}) e^{i\Phi_{\mathbf{q}}(\mathbf{k})\sigma\tau} \quad (\text{C3})$$

where $F_{\mathbf{q}}(\mathbf{k}) = |\lambda_{AA, +, \mathbf{q}}(\mathbf{k})|$ and $\phi_{\mathbf{q}}(\mathbf{k}) = \arg \lambda_{AA, +, \mathbf{q}}(\mathbf{k})$

We now investigate the Hartree-Fock solutions by looking for the minima of the Hartree-Fock energy. The Hartree-Fock energy is defined in terms of the order parameter

$$P_{\alpha\beta}(\mathbf{k}) = \langle c_\alpha^\dagger(\mathbf{k}) c_\beta(\mathbf{k}) \rangle \quad (\text{C4})$$

where α, β range over spin, valley and band indices. For an insulator or a semimetal, the number of filled states is \mathbf{k} independent and equal 4. This means that the order parameter $P_{\mathbf{k}}$ is a projector satisfying

$$P(\mathbf{k})^2 = P(\mathbf{k}) = P^\dagger(\mathbf{k}), \quad \text{tr } P(\mathbf{k}) = 4 \quad (\text{C5})$$

The Hartree-Fock energy can then be written as (using properties of the chiral limit)

$$E_{\text{HF}} = E_H + E_F, \quad (\text{C6})$$

$$E_H = \frac{1}{2A} \sum_{\mathbf{G}, \mathbf{k}, \mathbf{k}'} V_{\mathbf{G}} \text{tr } P(\mathbf{k}) \Lambda_{\mathbf{G}}^\dagger(\mathbf{k}) \text{tr } P(\mathbf{k}') \Lambda_{\mathbf{G}}(\mathbf{k}'), \quad (\text{C7})$$

$$E_F = -\frac{1}{2A} \sum_{\mathbf{q}, \mathbf{k}} V_{\mathbf{q}} \text{tr } P(\mathbf{k}) \Lambda_{\mathbf{q}}^\dagger(\mathbf{k}) P(\mathbf{k} + \mathbf{q}) \Lambda_{\mathbf{q}}(\mathbf{k}) \quad (\text{C8})$$

where we defined the form factor matrix $\Lambda_{\mathbf{q}}(\mathbf{k})$ in terms of the combined index $\alpha = (s, \tau, n)$ for spin, valley, and band as

$$\Lambda_{\mathbf{q}}(\mathbf{k}) = F_{\mathbf{q}}(\mathbf{k}) e^{i\Phi_{\mathbf{q}}(\mathbf{k})\sigma_z\tau_z} \quad (\text{C9})$$

The form factors decay in the separation \mathbf{q} with a characteristic scale which is typically smaller than the size of the Brillouin zone. This means that the sums in the Hartree and Fock terms are dominated by the $\mathbf{G} = 0$ term. For the Hartree term, this equals $4V(0)N$ and is independent of the order parameter $P(\mathbf{k})$. Thus, the Hartree term has little effect on the competition between different phases and will be neglected in the following.

We now consider possible types of symmetry-broken orders at charge neutrality. The order parameter $P(\mathbf{k})$ can generally be written as

$$P(\mathbf{k}) = \frac{1}{2}[1 + Q(\mathbf{k})], \quad \text{tr} Q(\mathbf{k}) = 0 \quad (\text{C10})$$

Since the Fock term is the largest contribution to the mean-field energy, let us now neglect the Hartree term as well as the single-particle term h_0 . We note that $\langle A, B \rangle = \text{tr} AB$ defines a positive definite inner product on the space of hermitian matrices. Using Cauchy-Schwarz inequality, we get

$$E_F \geq -\frac{1}{2A} \sum_{\mathbf{k}, \mathbf{q}} V_{\mathbf{q}} \sqrt{\text{tr} P(\mathbf{k}) \text{tr} [\Lambda_{\mathbf{q}}^\dagger(\mathbf{k}) P(\mathbf{k}') \Lambda_{\mathbf{q}}(\mathbf{k})]^2} = -\frac{2}{A} \sum_{\mathbf{k}, \mathbf{q}} V_{\mathbf{q}} F_{\mathbf{q}}^2(\mathbf{k}) \quad (\text{C11})$$

This inequality is satisfied if and only if $P(\mathbf{k} + \mathbf{q})$ is parallel to $\Lambda_{\mathbf{q}}(\mathbf{k}) P(\mathbf{k}) \Lambda_{\mathbf{q}}^\dagger(\mathbf{k})$ for every \mathbf{k}, \mathbf{q} . This means

$$P(\mathbf{k} + \mathbf{q}) = e^{i\Phi_{\mathbf{q}}(\mathbf{k})\sigma_z\tau_z} P(\mathbf{k}) e^{-i\Phi_{\mathbf{q}}(\mathbf{k})\sigma_z\tau_z} \Rightarrow Q(\mathbf{k} + \mathbf{q}) = e^{i\Phi_{\mathbf{q}}(\mathbf{k})\sigma_z\tau_z} Q(\mathbf{k}) e^{-i\Phi_{\mathbf{q}}(\mathbf{k})\sigma_z\tau_z} \quad (\text{C12})$$

1. Intervalley coherent states

Let us now briefly discuss states which break $U(1)$ valley symmetry. These states were argued to be energetically unfavorable in the context of twisted bilayer graphene with an aligned hBN substrate [37] and other Moiré materials which lack C_2 symmetry [17, 22]. Here, we will show that a similar argument fails [57] in C_2 -symmetric twisted bilayer graphene due to the extra particle-hole symmetry \mathcal{P} which is exact in the chiral limit. A more detailed discussion of such phases is provided in Ref. [50]. To clarify the importance of \mathcal{P} , we will assume that the symmetry is not present in which case, the form factors in the two opposite valleys at the same momentum \mathbf{k} are not related, i.e. $\lambda_{A/B,+, \mathbf{q}}(\mathbf{k}) \neq \lambda_{B/A, -, \mathbf{q}}(\mathbf{k})$. Furthermore, we will assume unbroken time-reversal symmetry. The case of time-reversal symmetry breaking can be addressed similarly. The projector for an IVC state can be split into a diagonal and off-diagonal component in valley space

$$P(\mathbf{k}) = P_d(\mathbf{k}) + P_o(\mathbf{k}), \quad P_d(\mathbf{k})^2 + P_o(\mathbf{k})^2 = P_d(\mathbf{k}), \quad (\text{C13})$$

In terms of valley resolved blocks of $P(\mathbf{k})$, i.e.

$$P = \begin{pmatrix} P_+ & P_{12} \\ P_{21} & P_- \end{pmatrix}, \quad (\text{C14})$$

the second condition can be written as

$$P_+^2 + P_{12}P_{21} = P_+, \quad P_-^2 + P_{21}P_{12} = P_-. \quad (\text{C15})$$

Since the form factors are diagonal in valley space, the Fock energy can be written as a sum of a term with only diagonal part and one with only off-diagonal parts as

$$\begin{aligned}
E_F &= -\frac{1}{2A} \sum_{\mathbf{k}, \mathbf{q}} V_{\mathbf{q}} \text{tr}[P_d(\mathbf{k})\Lambda_{\mathbf{q}}^\dagger(\mathbf{k})P_d(\mathbf{k} + \mathbf{q})\Lambda_{\mathbf{q}}(\mathbf{k}) + P_o(\mathbf{k})\Lambda_{\mathbf{q}}^\dagger(\mathbf{k})P_o(\mathbf{k} + \mathbf{q})\Lambda_{\mathbf{q}}(\mathbf{k})] \\
&\geq -\frac{1}{2A} \sum_{\mathbf{k}, \mathbf{q}} V_{\mathbf{q}} [|\lambda_{A,+,\mathbf{q}}(\mathbf{k})|^2 \sqrt{\text{tr} P_+(\mathbf{k})^2 \text{tr} P_+(\mathbf{k} + \mathbf{q})^2} + |\lambda_{A,-,\mathbf{q}}(\mathbf{k})|^2 \sqrt{\text{tr} P_-(\mathbf{k})^2 \text{tr} P_-(\mathbf{k} + \mathbf{q})^2} \\
&\quad + |\lambda_{A,+,\mathbf{q}}(\mathbf{k})||\lambda_{A,-,\mathbf{q}}(\mathbf{k})| \sqrt{\text{tr} P_o(\mathbf{k})^2 \text{tr} P_o(\mathbf{k} + \mathbf{q})^2}] \\
&\geq -\frac{1}{2A} \sum_{\mathbf{k}, \mathbf{q}} V_{\mathbf{q}} [|\lambda_{A,+,\mathbf{q}}(\mathbf{k})|^2 \text{tr} P_+(\mathbf{k})^2 + |\lambda_{A,-,\mathbf{q}}(\mathbf{k})|^2 \text{tr} P_-(\mathbf{k})^2 + |\lambda_{A,+,\mathbf{q}}(\mathbf{k})||\lambda_{A,-,\mathbf{q}}(\mathbf{k})| \text{tr} P_o(\mathbf{k})^2] \\
&= -\frac{1}{2A} \sum_{\mathbf{k}, \mathbf{q}} V_{\mathbf{q}} [|\lambda_{A,+,\mathbf{q}}(\mathbf{k})|^2 \text{tr}(P_+(\mathbf{k}) - P_{12}(\mathbf{k})P_{21}(\mathbf{k})) + |\lambda_{A,+,\mathbf{q}}(\mathbf{k})|^2 \text{tr}(P_-(\mathbf{k}) - P_{21}(\mathbf{k})P_{12}(\mathbf{k})) \\
&\quad + 2|\lambda_{A,+,\mathbf{q}}(\mathbf{k})||\lambda_{A,-,\mathbf{q}}(\mathbf{k})| \text{tr}(P_{12}(\mathbf{k})P_{21}(\mathbf{k}))] \\
&= -\frac{1}{A} \sum_{\mathbf{k}, \mathbf{q}} V_{\mathbf{q}} (|\lambda_{A,+,\mathbf{q}}(\mathbf{k})|^2 + |\lambda_{A,-,\mathbf{q}}(\mathbf{k})|^2) + \frac{1}{4A} \sum_{\mathbf{k}, \mathbf{q}} V_{\mathbf{q}} (|\lambda_{A,+,\mathbf{q}}(\mathbf{k})| - |\lambda_{A,-,\mathbf{q}}(\mathbf{k})|)^2 \text{tr} P_o(\mathbf{k})^2, \tag{C16}
\end{aligned}$$

Here, we used the Cauchy-Schwarz inequality to go from the first to the second line. We then used the geometric-arithmetic mean inequality $\sqrt{xy} \leq \frac{x+y}{2}$ to go from the second to the third. We now see that whenever the second term in the last line is non-zero, we would conclude that the Fock energy for the IVC is larger than the energy bound for the valley polarized or unpolarized phases by an amount which is proportional to the valley off-diagonal part of the order parameter. This energy difference in (C16) is generally not expected to be small unless there is a symmetry relating the same momenta in the two valleys (or equivalently a symmetry relating opposite momenta in the same valley). This is precisely the reason why the existence of particle-hole \mathcal{P} symmetry forces the second term to vanish which makes the bound (C16), while correct, inconclusive to rule out IVC states.

-
- [1] Yuan Cao, Valla Fatemi, Ahmet Demir, Shiang Fang, Spencer L Tomarken, Jason Y Luo, Javier D Sanchez-Yamagishi, Kenji Watanabe, Takashi Taniguchi, Efthimios Kaxiras, et al., “Correlated insulator behaviour at half-filling in magic-angle graphene superlattices,” *Nature* **556**, 80 (2018).
- [2] Yuan Cao, Valla Fatemi, Shiang Fang, Kenji Watanabe, Takashi Taniguchi, Efthimios Kaxiras, and Pablo Jarillo-Herrero, “Unconventional superconductivity in magic-angle graphene superlattices,” *Nature* **556**, 43 (2018).
- [3] Cenke Xu and Leon Balents, “Topological superconductivity in twisted multilayer graphene,” *Phys. Rev. Lett.* **121**, 087001 (2018).
- [4] Hoi Chun Po, LiuJun Zou, Ashvin Vishwanath, and T. Senthil, “Origin of mott insulating behavior and superconductivity in twisted bilayer graphene,” *Phys. Rev. X* **8**, 031089 (2018).
- [5] Hiroki Isobe, Noah F. Q. Yuan, and Liang Fu, “Unconventional superconductivity and density waves in twisted bilayer graphene,” *Phys. Rev. X* **8**, 041041 (2018).
- [6] Alex Thomson, Shubhayu Chatterjee, Subir Sachdev, and Mathias S. Scheurer, “Triangular antiferromagnetism on the honeycomb lattice of twisted bilayer graphene,” *Phys. Rev. B* **98**, 075109 (2018).
- [7] Yi-Zhuang You and Ashvin Vishwanath, “Superconductivity from valley fluctuations and approximate $so(4)$ symmetry in a weak coupling theory of twisted bilayer graphene,” arXiv preprint arXiv:1805.06867 (2018).
- [8] Jian Kang and Oskar Vafek, “Symmetry, maximally localized wannier states, and a low-energy model for twisted bilayer graphene narrow bands,” *Phys. Rev. X* **8**, 031088 (2018).
- [9] Ming Xie and Allan H MacDonald, “On the nature of the correlated insulator states in twisted bilayer graphene,” arXiv preprint arXiv:1812.04213 (2018).
- [10] Yu-Ping Lin and Rahul M Nandkishore, “A chiral twist on the high- T_c phase diagram in Moiré heterostructures,” arXiv preprint arXiv:1901.00500 (2019).
- [11] J. F. Dodaro, S. A. Kivelson, Y. Schattner, X. Q. Sun, and C. Wang, “Phases of a phenomenological model of twisted bilayer graphene,” *Phys. Rev. B* **98**, 075154 (2018).
- [12] Bikash Padhi, Chandan Setty, and Philip W Phillips, “Doped twisted bilayer graphene near magic angles: Proximity to wigner crystallization, not mott insulation,” *Nano letters* **18**, 6175–6180 (2018).
- [13] Fengcheng Wu, A. H. MacDonald, and Ivar Martin, “Theory of phonon-mediated superconductivity in twisted bilayer graphene,” *Phys. Rev. Lett.* **121**, 257001 (2018).
- [14] Biao Lian, Zhijun Wang, and B Andrei Bernevig, “Twisted bilayer graphene: A phonon driven superconductor,” arXiv preprint arXiv:1807.04382 (2018).
- [15] LiuJun Zou, Hoi Chun Po, Ashvin Vishwanath, and T. Senthil, “Band structure of twisted bilayer graphene: Emergent symmetries, commensurate approximants, and wannier obstructions,” *Phys. Rev. B* **98**, 085435 (2018).
- [16] Bitan Roy and Vladimir Juričić, “Unconventional superconductivity in nearly flat bands in twisted bilayer graphene,” *Phys. Rev. B* **99**, 121407 (2019).
- [17] Ya-Hui Zhang, Dan Mao, Yuan Cao, Pablo Jarillo-Herrero, and

- T. Senthil, “Nearly flat chern bands in moiré superlattices,” *Phys. Rev. B* **99**, 075127 (2019).
- [18] Eslam Khalaf, Alex J. Kruchkov, Grigory Tarnopolsky, and Ashvin Vishwanath, “Magic angle hierarchy in twisted graphene multilayers,” *Phys. Rev. B* **100**, 085109 (2019).
- [19] Christophe Mora, Nicolas Regnault, and B Andrei Bernevig, “Flat bands and perfect metal in trilayer moiré graphene,” arXiv preprint arXiv:1901.05469 (2019).
- [20] Tommaso Cea, Niels R Walet, and Francisco Guinea, “Twists and the electronic structure of graphitic materials,” arXiv preprint arXiv:1903.08403 (2019).
- [21] Zhen Bi, Noah FQ Yuan, and Liang Fu, “Designing flat band by strain,” arXiv preprint arXiv:1902.10146 (2019).
- [22] Jong Yeon Lee, Eslam Khalaf, Shang Liu, Xiaomeng Liu, Zeyu Hao, Philip Kim, and Ashvin Vishwanath, “Theory of correlated insulating behaviour and spin-triplet superconductivity in twisted double bilayer graphene,” *Nature Communications* **10**, 5333 (2019).
- [23] Matthew Yankowitz, Shaowen Chen, Hryhorii Polshyn, Yuxuan Zhang, K. Watanabe, T. Taniguchi, David Graf, Andrea F. Young, and Cory R. Dean, “Tuning superconductivity in twisted bilayer graphene,” *Science* **363**, 1059–1064 (2019), <https://science.sciencemag.org/content/363/6431/1059.full.pdf>.
- [24] Aaron L. Sharpe, Eli J. Fox, Arthur W. Barnard, Joe Finney, Kenji Watanabe, Takashi Taniguchi, M. A. Kastner, and David Goldhaber-Gordon, “Emergent ferromagnetism near three-quarters filling in twisted bilayer graphene,” arXiv e-prints, arXiv:1901.03520 (2019).
- [25] Xiaobo Lu, Petr Stepanov, Wei Yang, Ming Xie, Mohammed Ali Aamir, Ipsita Das, Carles Urgell, Kenji Watanabe, Takashi Taniguchi, Guangyu Zhang, Adrian Bachtold, Allan H. MacDonald, and Dmitri K. Efetov, “Superconductors, orbital magnets, and correlated states in magic angle bilayer graphene,” arXiv preprint arXiv:1903.06513 (2019).
- [26] Emilio Codecido, Qiyue Wang, Ryan Koester, Shi Che, Haidong Tian, Rui Lv, Son Tran, Kenji Watanabe, Takashi Taniguchi, Fan Zhang, et al., “Correlated insulating and superconducting states in twisted bilayer graphene below the magic angle,” arXiv preprint arXiv:1902.05151 (2019).
- [27] Guorui Chen, Aaron L Sharpe, Patrick Gallagher, Ilan T Rosen, Eli Fox, Lili Jiang, Bosai Lyu, Hongyuan Li, Kenji Watanabe, Takashi Taniguchi, et al., “Signatures of gate-tunable superconductivity in trilayer graphene/boron nitride moiré superlattice,” arXiv preprint arXiv:1901.04621 (2019).
- [28] Guorui Chen, Lili Jiang, Shuang Wu, Bosai Lyu, Hongyuan Li, Bheema Lingam Chittari, Kenji Watanabe, Takashi Taniguchi, Zhiwen Shi, Jeil Jung, Yuanbo Zhang, and Feng Wang, “Evidence of a gate-tunable mott insulator in a trilayer graphene moiré superlattice,” *Nature Physics* **15**, 237–241 (2019).
- [29] Xiaomeng Liu, Zeyu Hao, Eslam Khalaf, Jong Yeon Lee, Kenji Watanabe, Takashi Taniguchi, Ashvin Vishwanath, and Philip Kim, “Spin-polarized correlated insulator and superconductor in twisted double bilayer graphene,” arXiv:1903.08130 (2019).
- [30] Cheng Shen, Na Li, Shuopei Wang, Yanchong Zhao, Jian Tang, Jieying Liu, Jinpeng Tian, Yanbang Chu, Kenji Watanabe, Takashi Taniguchi, Rong Yang, Zi Yang Meng, Dongxia Shi, and Guangyu Zhang, “Observation of superconductivity with Tc onset at 12K in electrically tunable twisted double bilayer graphene,” arXiv e-prints, arXiv:1903.06952 (2019).
- [31] Yuan Cao, Daniel Rodan-Legrain, Oriol Rubies-Bigordà, Jeong Min Park, Kenji Watanabe, Takashi Taniguchi, and Pablo Jarillo-Herrero, “Electric Field Tunable Correlated States and Magnetic Phase Transitions in Twisted Bilayer-Bilayer Graphene,” arXiv e-prints, arXiv:1903.08596 (2019).
- [32] Rafi Bistritzer and Allan H. MacDonald, “Moiré bands in twisted double-layer graphene,” *Proceedings of the National Academy of Sciences* **108**, 12233–12237 (2011).
- [33] J. M. B. Lopes dos Santos, N. M. R. Peres, and A. H. Castro Neto, “Continuum model of the twisted graphene bilayer,” *Phys. Rev. B* **86**, 155449 (2012).
- [34] We follow the standard convention of measuring the filling relative to charge neutrality where the Dirac points of the original graphene sheet reside. Complete filling corresponds to $\nu_T = 4$ while completely empty $\nu_T = -4$ electrons per Moiré unit cell, accounting for both spin and valley degeneracy. Half filling corresponds to $\nu_T = \pm 2$.
- [35] Hoi Chun Po, Liu Jun Zou, T Senthil, and Ashvin Vishwanath, “Faithful tight-binding models and fragile topology of magic-angle bilayer graphene,” arXiv preprint arXiv:1808.02482 (2018).
- [36] A. O. Sboychakov, A. V. Rozhkov, A. L. Rakhmanov, and Franco Nori, “Many-body effects in twisted bilayer graphene at low twist angles,” *Phys. Rev. B* **100**, 045111 (2019).
- [37] Nick Bultinck, Shubhayu Chatterjee, and Michael P Zaletel, “Anomalous hall ferromagnetism in twisted bilayer graphene,” arXiv preprint arXiv:1901.08110 (2019).
- [38] Nguyen N. T. Nam and Mikito Koshino, “Lattice relaxation and energy band modulation in twisted bilayer graphene,” *Phys. Rev. B* **96**, 075311 (2017).
- [39] Mikito Koshino, Noah F. Q. Yuan, Takashi Koretsune, Masayuki Ochi, Kazuhiko Kuroki, and Liang Fu, “Maximally localized wannier orbitals and the extended hubbard model for twisted bilayer graphene,” *Phys. Rev. X* **8**, 031087 (2018).
- [40] Ya-Hui Zhang, Hoi Chun Po, and T Senthil, “Landau level degeneracy in twisted bilayer graphene: Role of symmetry breaking,” arXiv preprint arXiv:1904.10452 (2019).
- [41] Hoi Chun Po, Haruki Watanabe, and Ashvin Vishwanath, “Fragile topology and wannier obstructions,” *Phys. Rev. Lett.* **121**, 126402 (2018).
- [42] For semimetals, this is true everywhere except for the gapless points where the projector is not defined.
- [43] Youngjoon Choi, Jeannette Kemmer, Yang Peng, Alex Thomson, Harpreet Arora, Robert Polski, Yiran Zhang, Hechen Ren, Jason Alicea, Gil Refael, Felix von Oppen, Kenji Watanabe, Takashi Taniguchi, and Stevan Nadj-Perge, “Electronic correlations in twisted bilayer graphene near the magic angle,” *Nature Physics* **15**, 1174–1180 (2019).
- [44] Yuhang Jiang, Xinyuan Lai, Kenji Watanabe, Takashi Taniguchi, Kristjan Haule, Jinhai Mao, and Eva Y. Andrei, “Charge order and broken rotational symmetry in magic-angle twisted bilayer graphene,” *Nature* **573**, 91–95 (2019).
- [45] Alexander Kerelsky, Leo J. McGilly, Dante M. Kennes, Lede Xian, Matthew Yankowitz, Shaowen Chen, K. Watanabe, T. Taniguchi, James Hone, Cory Dean, Angel Rubio, and Abhay N. Pasupathy, “Maximized electron interactions at the magic angle in twisted bilayer graphene,” *Nature* **572**, 95–100 (2019).
- [46] Yonglong Xie, Biao Lian, Berthold Jäck, Xiaomeng Liu, Cheng-Li Chiu, Kenji Watanabe, Takashi Taniguchi, B. Andrei Bernevig, and Ali Yazdani, “Spectroscopic signatures of many-body correlations in magic-angle twisted bilayer graphene,” *Nature* **572**, 101–105 (2019).
- [47] Junyeong Ahn, Sungjoon Park, and Bohm-Jung Yang, “Failure of nielsen-ninomiya theorem and fragile topology in two-dimensional systems with space-time inversion symmetry: Application to twisted bilayer graphene at magic angle,” *Phys. Rev. X* **9**, 021013 (2019).
- [48] Biao Lian, Fang Xie, and B Andrei Bernevig, “The landau level

- of fragile topology,” arXiv preprint arXiv:1811.11786 (2018).
- [49] In general, the total second Stiefel-Whitney number of two isolated bands is not equal to the sum of the second Stiefel-Whitney numbers separately for the two bands; there is an additional contribution from the first Stiefel-Whitney classes. In the special case we considered here, the C_3 symmetry of the two-band subspace guarantees this additional term vanishes.
- [50] Nick Bultinck, Eslam Khalaf, Shang Liu, Shubhayu Chatterjee, Ashvin Vishwanath, and Michael P. Zaletel, “Ground state and hidden symmetry of magic angle graphene at even integer filling,” arXiv preprint arXiv:1911.xxxxx (2019).
- [51] We thank A. Thomson for correspondence on this point.
- [52] Grigory Tarnopolsky, Alex Jura Kruchkov, and Ashvin Vishwanath, “Origin of magic angles in twisted bilayer graphene,” Phys. Rev. Lett. **122**, 106405 (2019).
- [53] Alex Thomson and Jason Alicea, “Recovery of massless Dirac fermions at charge neutrality in strongly interacting twisted bilayer graphene with disorder,” arXiv preprint arXiv:1910.11348 (2019).
- [54] Notice that alternatively, if we choose a periodic gauge, α_{mk} can be made continuous but the Berry connection will be singular leading also to finite energy contribution.
- [55] The BM Hamiltonian has an approximate particle-hole symmetry at small angles.
- [56] Kasra Hejazi, Chunxiao Liu, Hassan Shapourian, Xiao Chen, and Leon Balents, “Multiple topological transitions in twisted bilayer graphene near the first magic angle,” Physical Review B **99**, 035111 (2019).
- [57] We thank Mike Zaletel for discussions on this point.